Inorganic Chemistry

Article

pubs.acs.org/IC

Hysteretic Spin Crossover in Two-Dimensional (2D) Hofmann-Type Coordination Polymers

Wei Liu,[†,▽] Lu Wang,[†,▽] Yu-Jun Su,[†] Yan-Cong Chen,[†] Jiri Tucek,[‡] Radek Zboril,[‡] Zhao-Ping Ni,*[,†] and Ming-Liang Tong*[,†]

[†]Key Laboratory of Bioinorganic and Synthetic Chemistry of Ministry of Education, School of Chemistry and Chemical Engineering, Sun Yat-Sen University, Guangzhou 510275, People's Republic of China

[‡]Regional Centre of Advanced Technologies and Materials, Departments of Physical Chemistry and Experimental Physics, Faculty of Science, Palacky University, Slechtitelu 27, 783 71 Olomouc, Czech Republic

Supporting Information

ABSTRACT: Three new two-dimensional (2D) Hofmann-type coordination polymers with general formula $[Fe(3\text{-}NH_2py)_2M(CN)_4]$ (3-NH_2py = 3-aminopyridine, M = Ni (**1**), Pd (**2**), Pt (**3**)) have been synthesized. Magnetic susceptibility measurements show that they exhibited cooperative spin crossover (SCO) with remarkable hysteretic behaviors. Their hysteresis widths are 25, 37, and 30 K for **1**−**3**, respectively. The single-crystal structure of **1** suggest that the pseudo-octahedral Fe sites are equatorially bridged by $[M(CN)_4]^{2-}$ to form 2D grids and axially coordinated by 3-NH_2py ligands. The intermolecular interactions between layers (the offset face-to-face $\pi\cdots\pi$ interactions, hydrogen bonds, and weak $N_{amino}\cdots Ni^{II}$ contacts) together with the covalent bonds bridged by $[M(CN)_4]^{2-}$ units are responsible to the significant cooperativity.

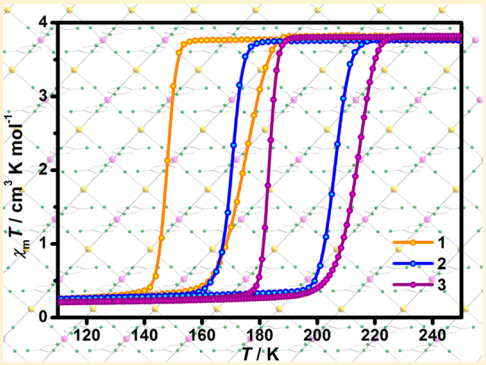

INTRODUCTION

Molecular switching materials have aroused great attention in materials science. The spin-crossover (SCO) complexes, in which the reversible conversion between high-spin (HS) and low-spin (LS) states can be triggered by an external perturbation (e.g., temperature, pressure, or light), represent one of the most attractive examples of switching materials.[1] An abrupt spin transition accompanied by large thermal hysteresis loop is deemed to be the prerequisite toward potential applications as data storage, display and switching devices, etc.[2] This means that strong cooperativity is needed throughout the solid lattice. In the last few decades, numerous spin-crossover materials have been synthesized and investigated to pursue strong SCO cooperativity. It is believed that the maximization of intermolecular interactions, such as $\pi\cdots\pi$ stacking, hydrogen bonds, could effectively enhance cooperativity in SCO compounds.[3] These subtle interactions often play a key role, but they are often difficult to control. In addition, another successful strategy reported to obtain strongly cooperative systems is the introduction of the SCO ions into coordination polymeric networks, in which the strong coordination bonding may strengthen the interactions between the spin transition centers.[2a,4] In this respect, some landmark achievements have been provided, such as one-dimensional (1D) iron(II)−triazole complexes[5] and two-dimensional (2D) or three-dimensional (3D) Hofmann-type coordination polymers.[6] The thermal hysteresis loops can routinely reach 20−40 K in the former case; however, their poorly crystalline weaknesses prevent the construction of structure−function relationships. For the classic Hofmann-type SCO coordination polymers, their equatorial positions of the [FeN6] sites are occupied by four CN groups from the tetracyanometalate bridging ligands, while the axial positions are linked by monodentate or *bis*-monodentate ligands into 2D/3D networks, suggesting the effectiveness in transmitting the SCO cooperativity.

The typical 3D porous Hofmann-type coordination polymers are $[Fe(pz)M(CN)_4]\cdot nH_2O$ (pz = pyrazine; M = Ni, Pd, or Pt), which can present ∼25 K hysteresis loops.[7] When the length of *bis*-monodentate ligands increases, their effectiveness of transmission of the cooperativity decrease if without thinking about the roles of guests in the pores.[8] The width of hysteresis loop had already decreased to zero when the organic pillar ligand was 1,4-bis(4-pyridylethynyl)benzene.[8e] Meanwhile, the 2D Hofmann-type coordination polymers $[Fe(py)_2M(CN)_4]$ could also exhibit relatively strong cooperativity (ΔT = 9 K), in which the weak $\pi-\pi$ interactions between pyridine rings belonging to adjacent layers were also involved, in addition to the transmission of SCO cooperativity through $[M(CN)_4]^{2-}$ units.[9] Most importantly, the substituent groups on the pyridine ligand have significant influences on the cooperativity.[10] The hysteresis widths were increased to 29, 35, and 26 K for $[Fe(3\text{-fluoropyridine})_2M(CN)_4]$ (M = Ni, Pd, and Pt),

Received: June 15, 2015
Published: August 10, 2015

DOI: 10.1021/acs.inorgchem.5b01341
Inorg. Chem. 2015, 54, 8711−8716

respectively. Moreover, unexpected large hysteresis loops (40 K) were found for $[Fe(4\text{-phenylpyridine})_2M(CN)_4]$ (M = Pd and Pt), in which the enhanced cooperativity results from the doubled $\pi-\pi$ interactions. Furthermore, these 2D Hofmann-type coordination polymers $[Fe(L)_2M(CN)_4]$ always pack densely without lattice solvent, which show encouraging stability favorable to application. Since the amino group has the ability to form rich intermolecular interactions, we choose the inexpensive 3-aminopyridine (3-NH_2py) as the monodentate ligand to pursue strong SCO cooperativity. Thus, three new 2D coordination polymers $[Fe(3\text{-}NH_2py)_2M(CN)_4]$ (M = Ni (**1**), Pd (**2**), and Pt (**3**)) have been synthesized and characterized. They all exhibit complete and abrupt spin transition behaviors with large thermal hysteresis loops. The hysteresis widths are 25, 37, and 30 K for **1**, **2**, and **3**, respectively.

EXPERIMENTAL SECTION

Materials and General Procedures. All the reagents and solvents employed were commercially available and used without further purification. All the synthesis were carried out under a nitrogen atmosphere to avoid oxidation of the Fe^{II} ion.

Synthesis of 1−3. The general procedures for the syntheses of powder samples of **1**−**3** are as follows. To 20 mL of mixed solvent of MeOH and H_2O (1:1), 39 mg of $(NH_4)_2Fe(SO_4)_2{\cdot}6H_2O$ (0.1 mmol) and 18 mg of 3-NH_2py (0.2 mmol) were added to form a pale blue precipitate immediately. Then, 10 mL of a water solution containing stoichiometric amounts of $K_2[Ni(CN)_4]$ (0.1 mmol; 24 mg) $K_2[Pd(CN)_4]$ (29 mg), and $K_2[Pt(CN)_4]$ (44 mg) was added under a nitrogen atmosphere. After 6 h, the precipitates were presented as light yellow powders. They then were filtered off, washed with H_2O and MeOH successively, and dried in a vacuum desiccator. Yield = 75% (**1**), 72% (**2**), and 81% (**3**). Elemental analysis for $C_{14}H_{12}FeN_8Ni$ (**1**) Calcd: C, 41.33; H, 2.97; N, 27.54; Found: C, 41.10; H, 3.13; N, 27.07. IR (KBr, cm^{-1}): 3442(m), 3363(m), 3215(w), 3082(w), 3045(w), 3024(w), 2150(s), 1616(s), 1578(s), 1489(m), 1445(s), 1356(w), 1292(m), 1266(w), 1197(w), 1139(w), 1054(w), 1080(w), 1022(w), 905(w), 853(w), 794(m), 694(s), 646(m), 545(w), 508(w), 434(s). Elemental analysis Calcd for $C_{14}H_{12}FeN_8Pd$ (**2**): C, 36.99; H, 2.66; N, 24.65; Found: C, 37.12; H, 2.80; N, 24.72. IR (KBr, cm^{-1}): 3446(m), 3368(m), 3214(w), 3084(w), 3049(w), 3026(w), 2167(s), 1929(w), 1618(s), 1582(s), 1489(m), 1446(s), 1353(w), 1292(m), 1265(w), 1199(w), 1137(w), 1055(w), 1024(w), 901(w), 852(w), 797(m), 696(m), 647(m), 544(w), 511(w), 413(m). Elemental analysis Calcd for $C_{14}H_{12}FeN_8Pt$ (**3**): C, 30.95; H, 2.23; N, 20.63; Found: C, 30.63; H, 2.17; N, 20.54. IR (KBr, cm^{-1}): 3445(m), 3365(m), 3213(w), 3079(w), 3047(w), 3021(w), 2167(s), 1929(w), 1616(s), 1580(s), 1491(m), 1441(s), 1352(w), 1290(m), 1263(w), 1200(w), 1137(w), 1052(w), 1026(w), 900(w), 851(w), 797(m), 694(m), 645(m), 543(w), 502(w), 453(m).

Single crystals of **1** were grown via the solvothermal method as follows. A glass tube with $K_2[Ni(CN)_4]$ (0.15 mmol, 0.036 g) in 1 mL H_2O was put into a 23 mL Teflon-lined reactor filled with 3-NH_2py (0.3 mmol, 0.027 g) and $FeSO_4{\cdot}7H_2O$ (0.1 mmol, 0.028 g) in EtOH/H_2O (5:4, 9 mL). It was heated at 120 °C for 3 days and then cooled to room temperature at −5 °C h^{-1}. Yellow quadrate crystals were obtained.

Physical Measurements. Powder X-ray diffraction (PXRD) patterns were performed on a Bruker Model D8 Avance X-ray diffractometer (Cu Kα, λ = 1.54056 Å) by scanning over the range of 5°−50°. The calculated patterns were generated using Mercury software. The Fourier transform infrared (FT-IR) spectra were recorded with KBr pellets in the range from 4000 cm^{-1} to 400 cm^{-1} with a Bruker Model EQUINOX 55 FT-IR spectrometer. The C, H, and N microanalyses were carried out with an Elementar Vario-ELCHNS elemental analyzer. TG analyses were carried out on a Netzsch Model TG209F3 thermoanalyzer under a nitrogen atmosphere at a heating rate of 10 K min^{-1}.

^{57}Fe Mössbauer spectra of the two samples were collected in the transmission geometry using a Mössbauer spectrometer operating at a constant acceleration mode and equipped with a 50 m Ci ^{57}Co (Rh) source. The sample was placed inside the chamber of the closed-helium cycle system with a nitrogen atmosphere inside. To fit the Mössbauer spectra, the MossWinn software program was used;[11] prior to fitting, the signal-to-noise ratio was adjusted by the filtering procedures built into the MossWinn software program and by using a statistically based approach developed by Prochazka et al.[12] The isomer shift values are referred metallic α-iron at room temperature.

Magnetic susceptibility measurements were measured on powder samples using a Quantum Design MPMS-XL SQUID susceptometer at 10−300 K with a rate of 2 K min^{-1} under an applied dc field of 1000 Oe. The Pascal constants were used for the diamagnetic corrections.

Differential scanning calorimetry (DSC) measurements were carried out on a TA Instruments Model DSC Q2000 system equipped with a liquid nitrogen cooling system (LNCS) in the temperature range of 120−300 K, at a rate of 10 K min^{-1}. The samples were placed in aluminum pans under a flow of dry helium. The data were analyzed with the Universal Analysis 2000 software.

Crystal Structure Determination. XRD data of **1** at 220 and 120 K were collected on an Oxford Diffraction Gemini R CCD system with Cu Kα radiation (λ = 1.54178 Å). All the structures were solved by a standard direct method. Least-squares on F^2 refinement were used with anisotropic thermal parameters for non-hydrogen atoms by the SHELXTL program.[13] Hydrogen atoms on 3-NH_2py were generated using the riding mode. DELU and ISOR commands are applied to amino group during refinement to fix the ADP and disorder problems. CCDC 1406025 (**1**-120 K) and 1406026 (**1**-220 K) contain the supplementary crystallographic data for this paper. These data can be obtained free of charge from The Cambridge Crystallographic Data Centre via www.ccdc.cam.ac.uk/data_request/cif.

RESULTS AND DISCUSSION

Crystal Structure. Most of the single crystals of Hofmann-type SCO coordination polymers were synthesized by slow-diffusion technique. Here, yellow single crystals of **1** were prepared using the solvothermal method unprecedentedly. The crystal structure was carried out at both 120 and 220 K. It crystallized in the monoclinic $C2/m$ space group under all of the applied temperatures. Tables 1 and 2 contain the crystallographic data and parameters recorded at these temperatures.

As shown in Figure 1, the X-ray crystal structures of **1** are similar to that of $[Fe(pyridine)_2Ni(CN)_4]$.[9] The asymmetric unit contains quarter of the formula, that is, a quarter of Fe^{II} ion, a quarter of $[Ni(CN)_4]^{2-}$ bridging ligand, and one-half of 3-NH_2py. Each Fe^{II} ion adopts a *trans* octahedral configuration: two N atoms from monodentate 3-NH_2py ligands in the axial positions and the others from four $[Ni(CN)_4]^{2-}$ in the equatorial positions. The coordination network is further connected by these bridging cyano ligands into undulating 2D [4,4] square grid parallel to the [010] plane (Figure 2). Furthermore, the sheets interdigitate in a stagger fashion such that the 3-NH_2py ligands align in an offset face to face fashion, further pack into a 3D dense-packed supramolecular structure. Thus, they generate offset $\pi\cdots\pi$ interactions, C−H···N hydrogen-bonding interactions, and unprecedented $N_{amino}\cdots Ni^{II}$ interactions between amino groups and coordinatively unsaturated Ni atoms. The distance between the centroids of pyridine rings is 3.61/3.71 Å at 120/220 K. The separation between two adjacent layers, measured from the plane defined by the Ni and Fe atoms, is 7.69 Å (120 K) [7.71 Å (220 K)]. The neighboring Fe···Fe distances through the $[Ni(CN)_4]^{2-}$ units are 6.96 and 7.07 Å (120 K) [7.21 and 7.25 Å (220 K)], while the shortest Fe···Fe path between the consecutive layers

DOI: 10.1021/acs.inorgchem.5b01341
Inorg. Chem. 2015, 54, 8711−8716

Table 1. Crystal Data for 1

parameter	Value/Comment	
	T = 120 K	T = 220 K
chemical formula	$C_{14}H_{12}FeN_8Ni$	$C_{14}H_{12}FeN_8Ni$
M_r	406.88	406.88
crystal system	monoclinic	monoclinic
space group	$C2/m$	$C2/m$
crystal size [mm]	0.24 × 0.17 × 0.12	0.24 × 0.17 × 0.12
a [Å]	15.5187(19)	15.8713(16)
b [Å]	6.9647(9)	7.2488(5)
c [Å]	7.0685(9)	7.2169(6)
β [°]	97.715(14)	103.731(11)
V [Å^3]	757.07(17)	806.56(12)
R_{int}	0.0306	0.0453
Z	2	2
ρ_{calcd} [g cm^{-3}]	1.785	1.675
$F(000)$	412.0	412.0
μ(Cu Kα) [mm^{-1}]	9.355	8.781
reflns collected	1915	1116
independent reflns	623	637
$R_1[I > 2(I)]$[a]	0.0489	0.0570
wR_2 [all data][b]	0.1320	0.1423
GOF	1.078	1.103

[a] $R_1 = \sum||F_0| - |F_c||/\sum|F_0|$. [b] $wR_2 = [\sum w(F_0^2 - F_c^2)^2/\sum w(F_0^2)^2]^{1/2}$.

Table 2. Selected Bond Lengths and Angles for 1

parameter	Value/Comment	
	T = 120 K	T = 220 K
Fe^{II} spin state	LS	HS
Σ (deg)	12.4	13.7
$\langle Fe-N\rangle_{average}$ (Å)	1.976(5)	2.161(7)
$\langle Fe-N_{ax}\rangle$ (Å)	2.020(5)	2.184(7)
$\langle Fe-N_{eq}\rangle$ (Å)	1.955(4)	2.149(5)

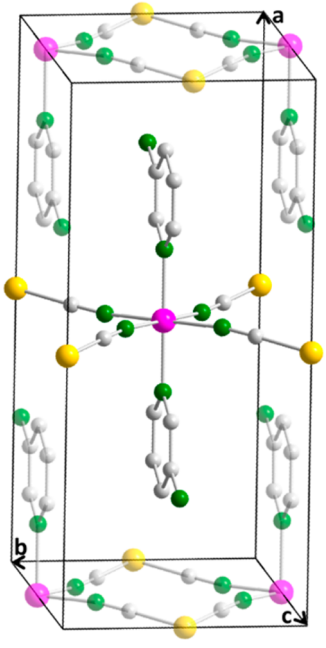

Figure 1. Crystal structures of **1** with coordination environments of Fe^{II} highlighted. [Atom code: Fe (pink), Ni (yellow), N (green), and C (gray).]

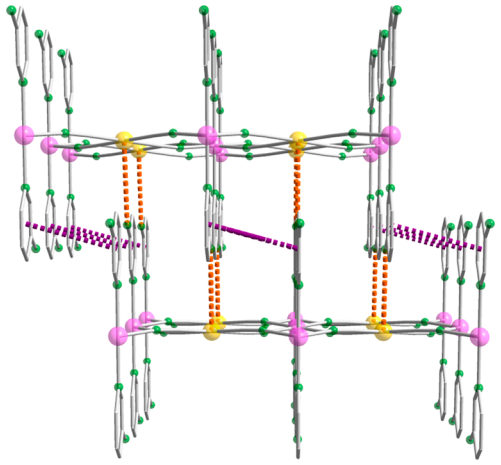

Figure 2. Side view of packing structure in **1**. Supramolecular interactions of two adjacent layers: offset face-to-face $\pi\cdots\pi$ and $N_{amino}\cdots Ni^{II}$ interactions are highlighted as purple and orange dashed lines, respectively. [Atom code: Fe (rose red), Ni (yellow), N (blue), and C (gray).]

is 8.50 Å (120 K) [8.72 Å (220 K)]. As shown in Figure S1 in the Supporting Information, hydrogen-bonding interaction is observed involving N_{amino} atom and hydrogen of the pyridine ring. The C···N distance and the C−H···N angle are 3.42/3.63 Å and 131.5°/121.6° at 120/220 K. Note that a weak van der Waals interaction between the N atom in the amino group and Ni atom in different layers is found and the $N_{amino}\cdots Ni^{II}$ separation is 3.66/3.99 Å at 120/220 K.

The bond lengths of Fe−N bonds are in the range of 1.95−2.02 Å at 120 K and increase to 2.15−2.19 Å at 220 K (Table 2), which are typical for iron(II) ion in LS and HS states, respectively. The coordination environment around Fe^{II} atoms at 220 K are more distorted than that at 120 K, which has a tendency to form a perfect octahedral configuration (octahedral distortion parameter, ΣFe-220 K: 13.7°, ΣFe-120 K: 12.4°).[14] The Fe−N≡C angle is 173.0° at 120 K and 164.8 at 220 K, respectively. The smaller deviation from 180° indicates a stronger σ-bond and hence a stronger ligand field strength. Unfortunately, until now, no single crystals of **2** and **3** have been obtained, despite the many attempts that have been made. PXRD studies on the powder sample of **1**−**3** have revealed their isostructural nature and shown the similar 2D structures based on $[FeM(CN)_4]$ units (see Figure S2 in the Supporting Information).

Magnetic Properties. Because of the high spin ($^5T_2$) to low spin ($^1A_1$) transition, the colors of the complexes **1**−**3** are yellow at room temperature and turn dark red at ∼80 K as emerged in liquid nitrogen (see Figure S3 in the Supporting Information). Variable-temperature magnetic susceptibility measurements have been served to monitor their SCO behavior directly. They are shown in Figure 3 in the form of $\chi_M T$ vs T plots (scan rate = 2 K min^{-1}), in which T is the absolute temperature and χ_M is the molar magnetic susceptibility. Detailing the magnetic curves of the Ni (**1**), Pd (**2**), and Pt (**3**) analogues shows that their magnetic behaviors are very similar. For **1**, the $\chi_M T$ values is equal to 3.77 cm^3 K mol^{-1} at 300 K, which corresponds to the high spin (HS) state of the Fe^{II} ions with S = 2. As the temperature decrease, the $\chi_M T$ value initially remains constant until T = 155 K, and then undergoes a rapid drop to 0.33 cm^3 K mol^{-1} at T = 140 K, representing a complete spin transition to LS state. The magnetic behavior

DOI: 10.1021/acs.inorgchem.5b01341
Inorg. Chem. 2015, 54, 8711−8716

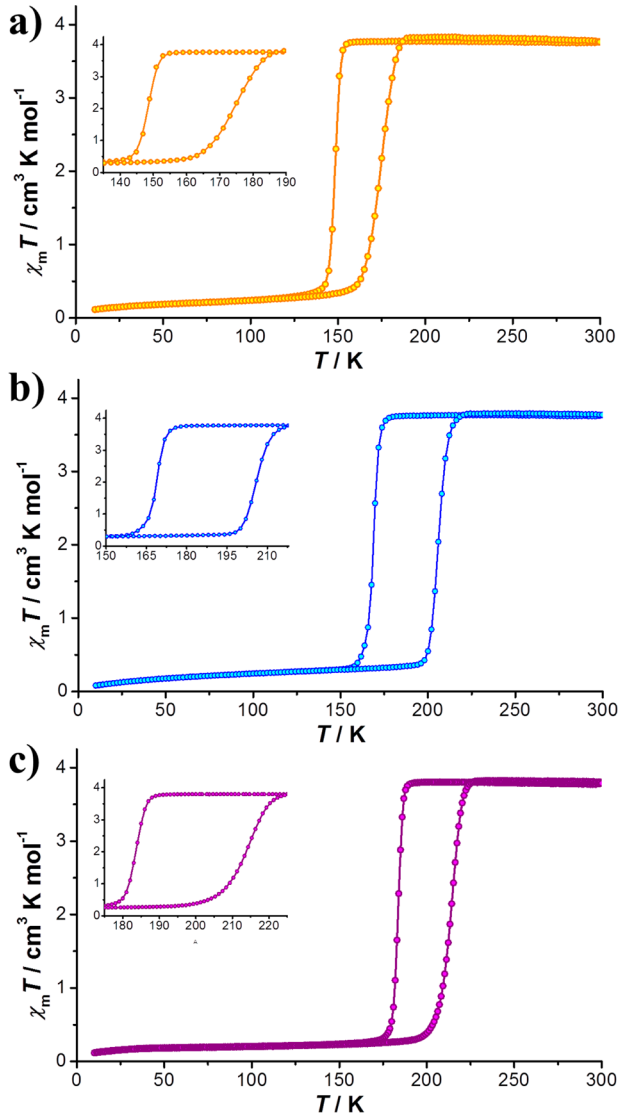

Figure 3. Magnetic properties of **1**−**3** in the form of $\chi_m T$ vs T. Data recorded in both cooling and heating modes at a scan rate of 2 K min^{-1}.

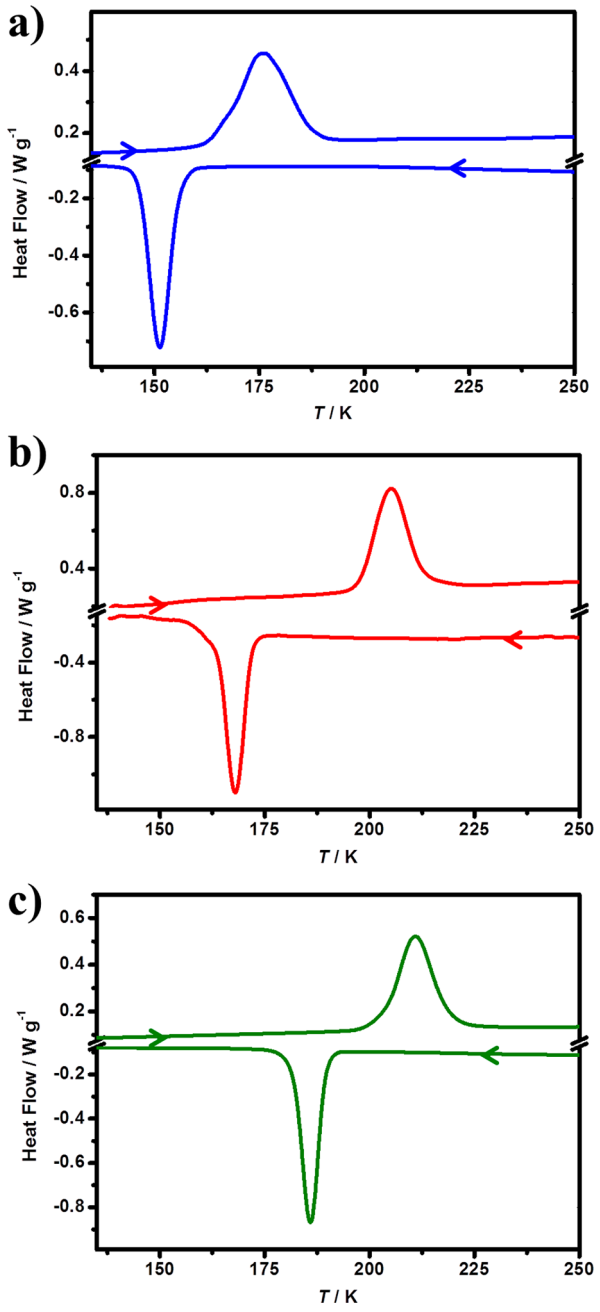

Figure 4. DSC measurements data for **1** (blue), **2** (red), and **3** (green).

with the subsequent heating mode defines a wide hysteresis loop (~25 K), with critical temperatures $T_c\downarrow$ = 148 K and $T_c\uparrow$ = 173 K. The $\chi_M T$ values in the high-temperature region are 3.75 and 3.83 cm^3 K mol^{-1} for **2** and **3**, and then diminish abruptly within a few Kelvin to 0.25 and 0.39 cm^3 K mol^{-1}, respectively. Their critical temperatures are $T_c\downarrow$ = 169 K, $T_c\uparrow$ = 206 K (ΔT = 37 K) for **2** and $T_c\downarrow$ = 183 K, $T_c\uparrow$ = 213 K (ΔT = 30 K) for **3**. One more cooling and warming thermal cycle of the magnetic response is shown in Figure S4 in the Supporting Information, demonstrating the reproducibility.[15]

Thermal Properties. Differential scanning calorimetry (DSC) measurements were carried out over the temperature range of 120−300 K at a rate of 10 K min^{-1}. Figure 4 shows the temperature dependence of the heat flow in both cooling and heating modes for **1**−**3**. The features in the cooling mode for **1** appear at $T_c\downarrow$ = 151 K and in the heating mode at $T_c\uparrow$ = 176 K, indicating the occurrence of hysteresis with a width of 25 K. Similarly, samples **2** and **3** exhibit anomalies at $T_c\downarrow$ = 168 K, $T_c\uparrow$ = 205 K for **2**, and $T_c\downarrow$ = 186 K, $T_c\uparrow$ = 211 K for **3**. These values are very consistent with the observation from the $\chi_M T$ vs T plots. The small differences between DSC and magnetic data in critical temperatures are caused by the different temperature controlling rates used in the experiments. The enthalpy (ΔH) and entropy (ΔS) variations are as follows: ΔH = 9.2 kJ mol^{-1} and ΔS = 60.7 J K^{-1} mol^{-1} (cooling mode), and ΔH = 10.0 kJ mol^{-1} and ΔS = 56.7 J K^{-1} mol^{-1} (heating mode) for **1**; ΔH = 13.8 kJ mol^{-1} and ΔS = 82.5 J K^{-1} mol^{-1} (cooling mode), and ΔH = 14.7 kJ mol^{-1} and ΔS = 71.7 J K^{-1} mol^{-1} (heating mode) for **2**; and ΔH = 13.1 kJ mol^{-1} and ΔS = 70.3 J K^{-1} mol^{-1} (cooling mode), and ΔH = 13.7 kJ mol^{-1} and ΔS = 65.2 J K^{-1} mol^{-1} (heating mode) for **3**. These thermodynamic parameters are consistent with the experimental range generally observed for Fe^{II} SCO compounds.[16]

^{57}Fe Mössbauer Spectroscopy. ^{57}Fe Mössbauer spectroscopy is a local sensitive probe that provides rich information on

DOI: 10.1021/acs.inorgchem.5b01341
Inorg. Chem. 2015, 54, 8711−8716

the Fe sites associated with the spin transition within a macroscopic powder sample. The spectra were collected at 100, 175, and 250 K for **1** and 150, 215, and 250 K for **3** in the cooling mode, respectively, to fully investigate the spin state and the corresponding transition process (see Figure 5, as well as Figure S5 in the Supporting Information and fitting parameters in Table S1). The spectra of sample **1** at 100 K and **3** at 150 K can be fitted with one singlet with an isomer shift value typical of Fe^{II} in a low spin state (for **1**, $S = 0$, $\delta = 0.48$; for **3**, $S = 0$, $\delta = 0.45$). The appearance of singlet implies that the electronic charge around the probed iron nucleus is of spherically symmetrical nature. The relatively narrow line width of the Mössbauer resonant line reflects a good crystallinity of the sample without any structural disorders or defects. At 175 K (for sample **1**), an additional doublet corresponding to HS Fe^{II} sites appears to show that partial Fe centers (36%; for **3** at 215 K, it is 39%) have undergone the LS → HS transition (LS Fe^{II}: $\delta = 0.44$; HS Fe^{II}: $\delta = 1.17$, $\Delta E_Q = 1.13$ mm s^{-1}; for **3**: LS Fe^{II}: $\delta = 0.47$; HS Fe^{II}: $\delta = 1.11$, $\Delta E_Q = 0.91$ mm s^{-1}). The spectrum of **1** at 250 K displays only one doublet characteristic a HS Fe^{II} species ($\delta = 1.10$, $\Delta E_Q = 0.89$ mm s^{-1}). However, the spectrum of **3** at 250 K also shows the two spectral components where the doublet significantly dominates (LS Fe^{II}: $\delta = 0.51$; HS Fe^{II}: $\delta = 1.10$, $\Delta E_Q = 0.92$ mm s^{-1}). The presence of the singlet implies that a very tiny portion (~7%) of Fe^{2+} ions still remain in the low-spin state. These results corroborate nicely with those obtained from the crystallographic data, as well as the magnetic analysis.

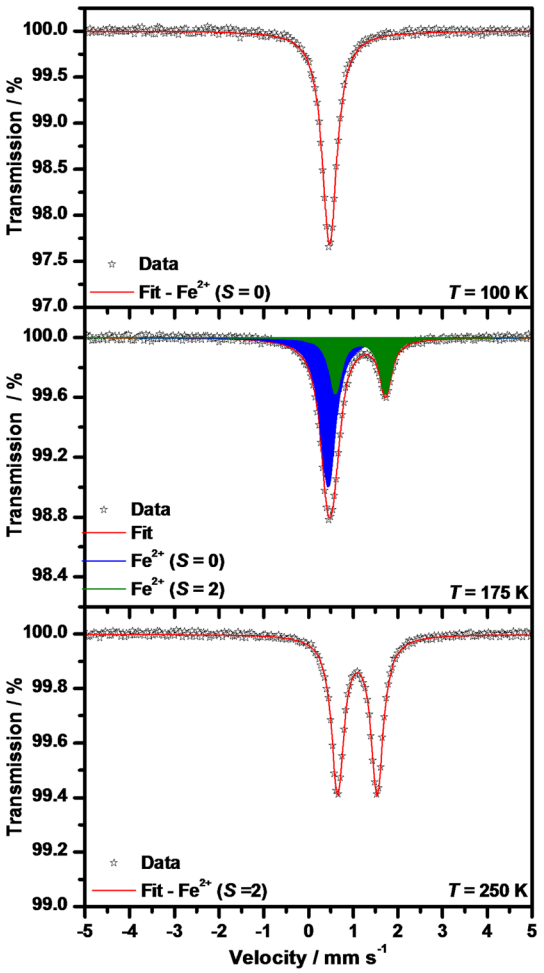

Figure 5. Mössbauer spectra of **1** (powder samples) recorded at various temperatures upon cooling.

DISCUSSION

The axial ligands in 2D Hofmann-type coordination polymer played a significant role in the SCO property, as shown in Table S2, which listed all the reported substituents located at meta-position on the pyridine ring. With the intention of exploring SCO materials with large hysteresis behaviors, we chose the monodentate 3-aminopyridine as the axial ligand to construct 2D Hofmann-type coordination polymers. They all showed complete and abrupt spin transition behaviors. Their critical transition temperatures revealed the following trend: **1** (148 and 173 K) < **2** (169 and 206 K) < **3** (183 and 213 K), which was consistent with former observations.[10] Most importantly, they undergo remarkable large hysteresis widths among the family of 2D Hofmann-type polymers. As shown in Table S2, the best reported SCO properties were found in $[Fe(3\text{-fluoropyridine})_2M(CN)_4]$, in which the hysteresis widths were 29, 35, and 26 K for Ni, Pd, and Pt, respectively, whereas the largest widths in original $[Fe(py)_2M(CN)_4]$ was only 9 K. Here, our hysteresis widths can reach 25, 37, and 30 K for **1**, **2**, and **3**, respectively. In addition to the common offset face-to-face $\pi\cdots\pi$ interactions based on the pyridine rings, the amino group should play key role in the enhanced SCO cooperativity. Similar to the F atom, the NH_2 group fill the channel more efficiently than the H atom. Hence, the internal pressure generated by the lattice can be transmitted more efficiently. In addition, the hydrogen-bonding interaction and unexpected $N_{amino}\cdots Ni^{II}$ interactions will also help to transmit the internal pressure, which should be responsible for the enhanced SCO cooperativity.

CONCLUSIONS

By using monodentate 3-aminopyridine as the axial ligand, three new 2D Hofmann-type SCO coordination polymers with the general formula $[Fe(3\text{-}NH_2py)_2M(CN)_4]$ (M = Ni (**1**), Pd (**2**), Pt (**3**)) were synthesized. The single crystals for **1** have been obtained by using the solvothermal method unprecedentedly. Most importantly, complexes **1**−**3** exhibited complete and abrupt SCO properties with remarkable 25, 37, and 30 K hysteresis loop widthes for **1**, **2**, and **3**, respectively, which will be in favor of practical applications. It was clear that, by introducing the amino group, the additional hydrogen-bonding interaction and unexpected $N_{amino}\cdots Ni^{II}$ interactions based on the original $[Fe(py)_2M(CN)_4]$ were responsible for the enhanced SCO cooperativity. Then, integrating functional groups into coordination polymers for transmitting cooperative interactions in SCO complexes are worthy of further investigation.

ASSOCIATED CONTENT

Supporting Information

The Supporting Information is available free of charge on the ACS Publications website at DOI: 10.1021/acs.inorgchem.5b01341.

Powder X-ray diffraction patterns, ^{57}Fe Mössbauer parameters, variable-temperature magnetic susceptibility studies of two successive thermal cycles (PDF)

Crystallographic information (CIF)

DOI: 10.1021/acs.inorgchem.5b01341
Inorg. Chem. 2015, 54, 8711−8716

AUTHOR INFORMATION

Corresponding Authors

*E-mail: nizhp@mail.sysu.edu.cn.
*E-mail: tongml@mail.sysu.edu.cn.

Author Contributions

[∇]These authors contributed equally to this work

Notes

The authors declare no competing financial interest.

ACKNOWLEDGMENTS

This work was supported by the "973 Project" (Nos. 2012CB821704 and 2014CB845602), the NSFC (Grant Nos. 91122032, 21201182, 21373279, and 91422302), and the Program for Changjiang Scholars and Innovative Research Team in University, China.

REFERENCES

(1) (a) Kahn, O.; Martinez, C. J. *Science* **1998**, *279*, 44−48. (b) Gütlich, P.; Goodwin, H. A. *Top. Curr. Chem.* **2004**, *233*, 1−47. (c) Murray, K. S. *Spin-Crossover Materials: Properties and Applications*; Halcrow, M. A., Ed.; Wiley: Chichester, U.K., 2013; Chapter 1, pp 1−54 10.1002/9781118519301.ch1 (d) Halcrow, M. A. *Chem. Soc. Rev.* **2011**, *40*, 4119−4142. (e) Gütlich, P.; Gaspar, A. B.; Garcia, Y. *Beilstein J. Org. Chem.* **2013**, *9*, 342−391.

(2) (a) Bousseksou, A.; Molnár, G.; Salmon, L.; Nicolazzi, W. *Chem. Soc. Rev.* **2011**, *40*, 3313−3335. (b) Létard, J.-F.; Guionneau, P.; Goux-Capes, L. *Top. Curr. Chem.* **2004**, *235*, 221−249. (c) Coronado, E.; Minguez Espallargas, G. *Chem. Soc. Rev.* **2013**, *42*, 1525−1539. (d) Sato, O.; Tao, J.; Zhang, Y.-Z. *Angew. Chem., Int. Ed.* **2007**, *46*, 2152−2187.

(3) (a) Halcrow, M. A. *Spin-Crossover Materials: Properties and Applications*; Halcrow, M. A., Ed.; Wiley: Chichester, U.K., 2013; Chapter 5, pp 147−169 10.1002/9781118519301.ch5 (b) Weber, B.; Bauer, W.; Obel, J. *Angew. Chem., Int. Ed.* **2008**, *47*, 10098−10101.

(4) (a) Weber, B. *Coord. Chem. Rev.* **2009**, *253*, 2432−2449. (b) Murray, K. S.; Kepert, C. J. *Top. Curr. Chem.* **2004**, *233*, 195−228.

(5) (a) Roubeau, O. *Chem.—Eur. J.* **2012**, *18*, 15230−15244. (b) Aromí, G.; Barrios, L. A.; Roubeau, O.; Gamez, P. *Coord. Chem. Rev.* **2011**, *255*, 485−546.

(6) (a) Muñoz, M. C.; Real, J. A. *Coord. Chem. Rev.* **2011**, *255*, 2068−2093. (b) Muñoz, M. C.; Real, J. A. *Spin-Crossover Materials: Properties and Applications*; Halcrow, M. A., Ed.; Wiley: Chichester, U.K., 2013; Chapter 4, pp 121−146 10.1002/9781118519301.ch4

(7) Niel, V.; Martinez-Agudo, J. M.; Munoz, M. C.; Gaspar, A. B.; Real, J. A. *Inorg. Chem.* **2001**, *40*, 3838−3839.

(8) (a) Sciortino, N. F.; Scherl-Gruenwald, K. R.; Chastanet, G.; Halder, G. J.; Chapman, K. W.; Letard, J. F.; Kepert, C. J. *Angew. Chem., Int. Ed.* **2012**, *51*, 10154−10158. (b) Sciortino, N. F.; Neville, S. M.; Letard, J. F.; Moubaraki, B.; Murray, K. S.; Kepert, C. J. *Inorg. Chem.* **2014**, *53*, 7886−7893. (c) Munoz-Lara, F. J.; Gaspar, A. B.; Munoz, M. C.; Arai, M.; Kitagawa, S.; Ohba, M.; Real, J. A. *Chem.—Eur. J.* **2012**, *18*, 8013−8018. (d) Agusti, G.; Cobo, S.; Gaspar, A. B.; Molnár, G. b.; Moussa, N. O.; Szilágyi, P. Á.; Pálfi, V.; Vieu, C.; Carmen Muñoz, M.; Real, J. A.; Bousseksou, A. *Chem. Mater.* **2008**, *20*, 6721−6732. (e) Muñoz-Lara, F. J.; Gaspar, A. B.; Muñoz, M. C.; Ksenofontov, V.; Real, J. A. *Inorg. Chem.* **2013**, *52*, 3−5. (f) Bartual-Murgui, C.; Salmon, L.; Akou, A.; Ortega-Villar, N. A.; Shepherd, H. J.; Muñoz, M. C.; Molnár, G.; Real, J. A.; Bousseksou, A. *Chem.—Eur. J.* **2012**, *18*, 507−516. (g) Bartual-Murgui, C.; Ortega-Villar, N. A.; Shepherd, H. J.; Muñoz, M. C.; Salmon, L.; Molnár, G.; Bousseksou, A.; Real, J. A. *J. Mater. Chem.* **2011**, *21*, 7217−7222. (h) Ohtani, R.; Arai, M.; Hori, A.; Takata, M.; Kitao, S.; Seto, M.; Kitagawa, S.; Ohba, M. *J. Inorg. Organomet. Polym. Mater.* **2013**, *23*, 104−110. (i) Pineiro-Lopez, L.; Seredyuk, M.; Munoz, M. C.; Real, J. A. *Chem. Commun.* **2014**, *50*, 1833−1835.

(9) Kitazawa, T.; Gomi, Y.; Takahashi, M.; Takeda, M.; Enomoto, M.; Miyazaki, A.; Enoki, T. *J. Mater. Chem.* **1996**, *6*, 119−121.

(10) (a) Martínez, V.; Gaspar, A. B.; Muñoz, M. C.; Bukin, G. V.; Levchenko, G.; Real, J. A. *Chem.—Eur. J.* **2009**, *15*, 10960−10971. (b) Martínez, V.; Gaspar, A. B.; Muñoz, M. C.; Ballesteros, R.; Ortega-Villar, N.; Ugalde-Saldívar, V. M.; Moreno-Esparza, R.; Real, J. A. *Eur. J. Inorg. Chem.* **2009**, *2009*, 303−310. (c) Molnár, G.; Guillon, T.; Moussa, N. O.; Rechignat, L.; Kitazawa, T.; Nardone, M.; Bousseksou, A. *Chem. Phys. Lett.* **2006**, *423*, 152−156. (e) Agustí, G.; Gaspar, A. B.; Muñoz, M. C.; Real, J. A. *Inorg. Chem.* **2007**, *46*, 9646−9654. (e) Martínez, V.; Boldog, I.; Gaspar, A. B.; Ksenofontov, V.; Bhattacharjee, A.; Gütlich, P.; Real, J. A. *Chem. Mater.* **2010**, *22*, 4271−4281. (f) Kitazawa, T.; Eguchi, M.; Takeda, M. *Mol. Cryst. Liq. Cryst. Sci. Technol., Sect. A* **2000**, *341*, 527−532.

(11) Klencsar, Z.; Kuzmann, E.; Vertes, A. *J. Radioanal. Nucl. Chem.* **1996**, *210*, 105−118.

(12) Prochazka, R.; Tucek, P.; Tucek, J.; Marek, J.; Mashlan, M.; Pechousek, J. *Meas. Sci. Technol.* **2010**, *21*, 025107.

(13) (a) Sheldrick, G. M. *XPREP. Space Group Determination and Reciprocal Space Plots*; Siemens Analytical X-ray Instruments: Madison, WI, 1991 (b) Sheldrick, G. M. *Acta Crystallogr., Sect. A: Found. Crystallogr.* **2008**, *A64*, 112−122.

(14) Guionneau, P.; Brigouleix, C.; Barrans, Y.; Goeta, A. E.; Létard, J. F.; Howard, J. A. K.; Gaultier, J.; Chasseau, D. *C. R. Acad. Sci., Ser. IIc: Chim.* **2001**, *4*, 161−171.

(15) Brooker, S. *Chem. Soc. Rev.* **2015**, *44*, 2880−2892.

(16) (a) Šalitroš, I.; Madhu, N.; Boča, R.; Pavlik, J.; Ruben, M. *Monatsh. Chem.* **2009**, *140*, 695−733. (b) Sorai, M.; Nakano, M.; Miyazaki, Y. *Chem. Rev.* **2006**, *106*, 976−1031.

DOI: 10.1021/acs.inorgchem.5b01341
Inorg. Chem. 2015, 54, 8711−8716